### Title
Enhanced interfacial ferromagnetism and exchange bias in (111)-oriented LaNiO3/CaMnO3 superlattices




### Journal
Physical Review Materials, 3(6)

### ISSN
2476-0455



### Authors
Flint, CL
Yi, D
Karapetrova, E
et al.



### Publication Date
2019-06-01

### DOI
10.1103/physrevmaterials.3.064401

Peer reviewed

# Enhanced interfacial ferromagnetism and exchange bias in (111)-oriented $LaNiO_3$/$CaMnO_3$ superlattices

C. L. Flint,[1,2] D. Yi,[2] E. Karapetrova,[3] A. T. N'Diaye,[4] P. Shafer,[4] E. Arenholz,[4] and Y. Suzuki[2,5]

[1]*Department of Materials Science and Engineering, Stanford University, Stanford, California 94305, USA*

[2]*Geballe Laboratory for Advanced Materials, Stanford University, Stanford, California 94305, USA*

[3]*Advanced Photon Source, Argonne National Laboratory, Argonne, Illinois 60439, USA*

[4]*Advanced Light Source, Lawrence Berkeley National Laboratory, Berkeley, California 94720, USA*

[5]*Department of Applied Physics, Stanford University, Stanford, California 94305, USA*

Emergent properties of complex oxide interfaces are based on interface reconstruction that is driven by mismatch of electronic bands, valence states, interaction lengths, and even crystal symmetry of the interface. In particular, emergent ferromagnetism at the interface of two materials that do not exhibit ferro- or ferrimagnetism in the bulk has been stabilized as a result of competing exchange interactions. When $LaNiO_3$ and $CaMnO_3$, which are a paramagnetic metal and antiferromagnetic insulator in the bulk, respectively, are brought together, ferromagnetism emerges at the interface. Here we show that in (111)-oriented $LaNiO_3$/$CaMnO_3$ (LNO/CMO) superlattices, $Ni^{2+}$-$Mn^{4+}$ superexchange interactions due to polar mismatch at the LNO/CMO interfaces are responsible for the emergent ferromagnetism. Compared to (001)-oriented LNO/CMO superlattices, (111)-oriented LNO/CMO superlattices exhibit enhanced interfacial ferromagnetism with a $T_C$ > 200 K, greater than the bulk antiferromagnetic transition temperature of $CaMnO_3$ and a saturated magnetic moment enhanced by up to a factor of 3. Furthermore, we observe exchange bias in (111)-oriented superlattices. The strong exchange interactions along the (111) interface, manifest in the enhanced $T_c$ and exchange bias, make this class of CMO-based materials with (111)-oriented interfaces good candidates for low-dimensional spin-polarized materials in spintronic applications.

## I. INTRODUCTION

Emergent ferromagnetic phenomena at interfaces, where the constituent materials are not ferromagnetic, have been of fundamental and technological interest as they provide model systems for low-dimensional magnetism. Perovskite oxide heterostructures have been of particular interest as atomically precise interfaces have been realized routinely and perovskite oxides can be stabilized in a variety of magnetic ground states. The emergent ferromagnetism has been driven by mismatch of electronic bands, valence states, interaction lengths, and even crystal symmetry depending on the constituent materi- als. For example, emergent ferromagnetism has been gener- ated in a single unit cell at the interfaces of (001)-oriented $CaMnO_3$/$CaRuO_3$ (CMO/CRO) superlattices and is believed to arise from a double exchange interaction due to the leakage of itinerant electrons from the CRO into the interface CMO layer [1–5]. This results in a ferromagnetic interface layer that is adjacent and exchange biased to the rest of the antifer- romagnetic CMO [4,5]. In (001)-oriented $LaNiO_3$/$CaMnO_3$ (LNO/CMO) superlattices, composed of CMO and LNO that are antiferromagnetic and paramagnetic, respectively, in the bulk, emergent ferromagnetism has also been observed. In addition to the double exchange interactions, which are caused by the leakage of electrons into the CMO layer, polar and crystal symmetry mismatch at the interfaces provides driving forces toward the stabilization of a ferromagnetic ground state at the interfaces of LNO/CMO superlattices [6,7]. This polar

mismatch results in the formation of $Ni^{2+}$ that compensates for the polar discontinuity in LNO/CMO superlattices, but only when it is present at the interface [6]. The presence of interfacial $Ni^{2+}$ and $Mn^{4+}$ gives rise to ferromagnetism due to a $Ni^{2+}$-$Mn^{4+}$ superexchange interaction, as revealed in prior work [6,7]. In contrast, bulk ferromagnets that are reduced to thin films that are just a few unit cells thick often cannot stabilize long-range magnetic order [8].

With advances in the growth of perovskite oxide thin films and especially superlattices, the opportunity for exploring these oxide materials at higher-energy surfaces and interfaces has led to the discovery of new emergent and exotic states. Low-dimensional (111)-oriented heterostructures have been identified as possible candidates for nontrivial band topology as well as nontrivial magnetic ground states. For example, Ueda *et al.* found that (111)-oriented $(LaCrO_3)_1/(LaFeO_3)_1$ superlattices exhibited ferromagnetism that can be ex- plained in terms of the Goodenough-Kanemori rules [9]. In $LaNiO_3$/$LaMnO_3$ (LNO/LMO) superlattices composed of weakly ferromagnetic LMO and paramagnetic LNO in the bulk, Gibert *et al.* found that (111)-oriented superlattices exhibited a unique spin helical structure with exchange bias of the ferromagnetic LMO layers [10]. In addition to favoring exchange bias, the (111)-growth orientation may enhance interfacial ferromagnetism due to the largely uncompensated (111) CMO spin structure and increased number of interfacial bonds (see Fig. 1).

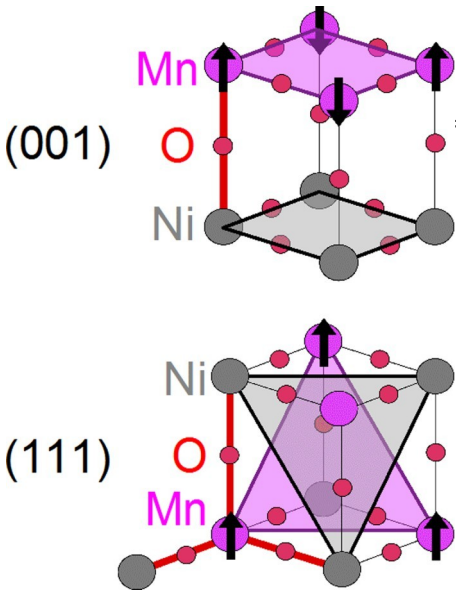


FIG. 1. Schematic of $M_1$-O-$M_2$ bonding across the interface in (1) (a) and (111) (b) orientations, using Ni and Mn as an example. (111)-oriented superlattices have three times as many $M_1$-O-$M_2$ interfacial bonds and a completely uncompensated spin structure (all spins pointing in the same direction) along the (111) surface in contrast to the completely compensated spin structure (net spin is zero) along the (001) surface. Adapted from Kim *et al.* [11].

In this paper, we demonstrate that the (111)-oriented LNO/CMO interface gives rise to strong interfacial ferro- magnetism based on $Ni^{2+}$-$Mn^{4+}$ superexchange interactions associated with screening effects caused by polar mismatch. The (111) interface maximizes emergent interfacial moments and exchange interactions. These experiments are possible due to our recent success in synthesizing atomically precise LNO/CMO superlattices with (111) orientation by interval pulsed laser deposition [12]. The (111) interface gives rise to strong exchange interactions, beyond those found in (001) LNO/CMO superlattices, resulting in a ferromagnetic order- ing temperature of 200 K, which is much higher than the bulk antiferromagnetic CMO ordering temperature of 140 K. The significant saturated interfacial moment is attributed to the fully uncompensated (111) CMO surface. Fully uncom- pensated spin structures refer to orientations within antifer- romagnets where all of the spins along that plane point in the same direction. The strong exchange interaction in our superlattices grown along the (111) direction [hereafter re- ferred to as (111)-oriented superlattices] is also manifest in the observed exchange bias associated with the coupling between the interfacial CMO and the interior antiferromagnetic (AFM) CMO.

## II. EXPERIMENT

To explore interface ferromagnetism at (111) interfaces, $[(LNO)_N/(CMO)_{M=4}]_{P=10}$ superlattices were synthesized on (111)-oriented $LaAlO_3$ (LAO) single-crystal substrates using pulsed laser deposition. $N$ was varied from $N$ 2 to 10, where $N$ is even (e.g., 2, 4, ... ). $M$ was held constant at 4. The superlattice period was repeated ten times. Note that LNO is

rhombohedral with a pseudocubic lattice parameter of 3.85 Å [13], while CMO is orthorhombic with a pseudocubic lattice parameter of 3.73 Å [14]. This gives (111) planar distances of
2.22 Å for LNO and 2.15 Å for CMO. On LAO (pseudocubic lattice parameter of 3.79 Å), this results in a tensile strain of 1.6% for CMO and a compressive strain of 1.6% for LNO. Films were deposited using a 248 nm KrF laser at 1 Hz with a fluence of 1.3 J/cm$^2$. The substrate was heated to 780 °C in an atmosphere of 30 mTorr of $O_2$. To improve superlattice uniformity, superlattices were deposited using an interval deposition method [12,15]. In this deposition method, one unit cell of material was deposited at a laser repetition rate of 10 Hz, followed by full recovery of the reflective high-energy electron diffraction (RHEED) intensity before the next unit cell was deposited.

## III. RESULTS

X-ray diffraction (XRD) and x-ray reflectivity (XRR) measurements were performed to characterize the superlat- tice structure. XRD was performed at sector 33-BM at the Advanced Photon Source at Argonne National Laboratory while XRR was performed on a PANalytical X'Pert Pro system at Stanford University. XRR results are presented in Fig. 2(a) and offset for clarity, while XRD results are shown in Fig. 2(b). Superlattice satellite peaks and thickness fringes are observable for all superlattices in XRR and XRD. Superlattice thickness was determined via calibration of film growth rates using test depositions (see the Supplemental Material [16] for more information on growth calibrations). All superlattices show the expected number ($P$ 2 8) of thickness fringes for $P$ 10 superlattice periods. Roughness was determined by atomic force microscopy to be 0.2 nm for $N$ 2–4 up to 0.5 nm in $N$ 6–10 superlattices (see the Supplemental Material [16] for atomic force microscopy). This increased roughness results in diminished superlattice thickness fringes after the first superlattice satellite peaks in XRD as seen in Fig. 2(b). In particular, for the $N$ 10 superlattice, sig- nificant roughness can be seen from the broadening of the
(2) Bragg peak in XRR. However, the clear observation
of superlattice thickness fringes for all superlattices indicates that the superlattice layers are reasonably smooth. Thus x-ray characterization and atomic force microscopy indicate that all superlattices exhibit distinct and smooth layering for all superlattice periods despite the increasing roughness with increasing LNO layer thickness.

It has been reported that the metal-insulator transition of rare-earth nickelates is sensitive to growth orientation, possibly due to the effects of oxygen octahedral rotation at the interface with the substrate [17,18]. Since the trans- port reflects the electronic structure, which in turn affects the emergent magnetism, we have investigated the temper- ature dependence of the resistivity from 10 to 300 K as shown in Fig. 3(a). Superlattices with $N < 10$ are clearly insulating while the resistivity of the $N \sim 10$ superlattice is nearly temperature-independent. The weak minimum at $T$ 200 K may be consistent with the previously observed weak localization effects in LNO thin films [19]. The increased resistivity for (111)-oriented superlattices, relative to the (001) superlattices, while possibly expected for the higher-energy

− =

=

=

=

=

=

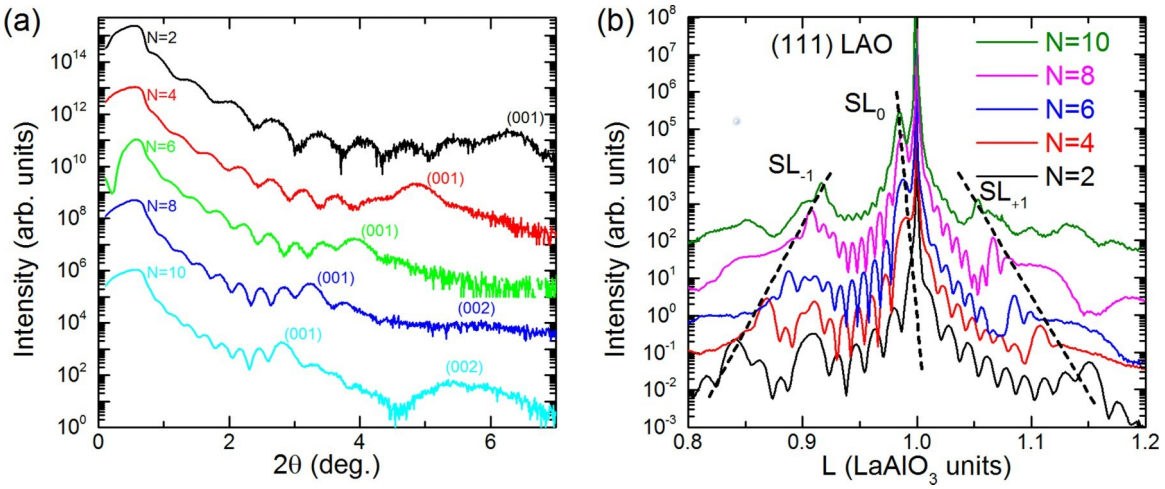


FIG. 2. (a) X-ray reflectivity scans for all $N$ 2, 4,..., 10 superlattices offset for clarity. Superlattice Bragg peaks are indexed. (b) X-ray diffraction around the (111) $LaAlO_3$ substrate peak. (111) Bragg peaks, thickness fringes, and superlattice satellite peaks are clearly visible for all superlattices except the (111) Bragg peak of $N$ = 2, which is obscured by the substrate peak.

(111) surface, may also be related to increased $Ni^{2+}$ due to the highly polar (111) interface [20]. Therefore, testing this hypothesis is warranted.

To probe the Ni cation valence, x-ray absorption spec- troscopy (XAS) measurements were performed in total elec- tron yield at 30° grazing at beamline 4.0.2 of the Advanced Light Source. XAS was performed at 300 K. The results are presented in Fig. 3(b). The Ni $L_3$ edge overlaps with the strong absorption intensity of the La $M_4$ peak and therefore care must be taken to subtract the La $M_4$ edge from XAS data to reveal the Ni $L_3$ edge. To perform a direct comparison of the Ni $L_3$ edge peaks for varying LNO layer thickness, we normalized the La $M_4$ peak height to the same intensity and then fit the La $M_4$ edge with a combined Lorentzian and Gaussian expres- sion, which was subsequently subtracted from the normalized data (see the Supplemental Material [16] for details on La $M_4$ edge subtraction). For comparison, we also plot the Ni XAS of a 12-nm-thick film in Fig. 3(b) which is representative of $Ni^{3+}$ spectra. The presence of $Ni^{2+}$ is represented in a narrow absorption feature around 853 eV at the $L_3$ edge and with a double-peak feature at the $L_2$ edge as seen in NiO reference spectra [6]. It is apparent that the thinner superlattices have a significant fraction of $Ni^{2+}$, consistent with our previous results in (001)-oriented superlattices [6]. As in the (001)-oriented superlattices, the $Ni^{2+}$ content diminishes as the LNO thickness increases. In (001)-oriented superlattices, the $Ni^{2+}$ content was indiscernible using XAS for $N$ ≤ 6 due to the decreasing $Ni^{2+}/Ni^{3+}$ ratio [6]. However, in these (111)-oriented superlattices, it is evident that $Ni^{2+}$ is present in a small fraction even for the $N$ = 10 superlattice. The fact that $Ni^{2+}$ XAS is observable in the thicker (111)-oriented superlattices is the result of a greater $Ni^{2+}$ fraction in the (111)-oriented $N$ ≤ 6 superlattices compared to the (001) $N$ ≤ 6 superlattices. This is attributed to interface charge redistribution caused by polar mismatch at the LNO/CMO interfaces [16,21,22]. Prior research on LNO/LMO has also

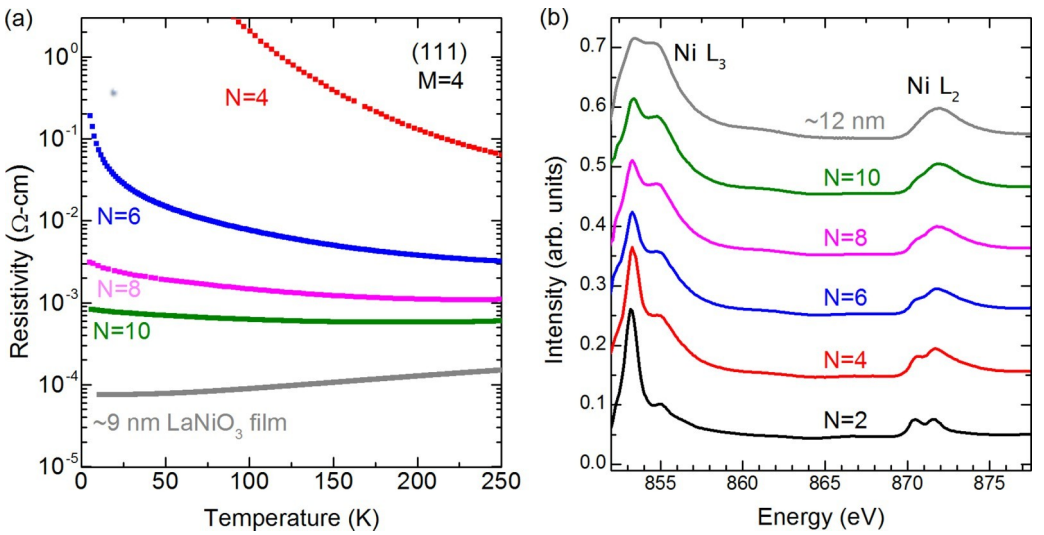

FIG. 3. (a) Resistivity vs temperature from 5 to 250 K. A 9 nm $LaNiO_3$ film is included for comparison. (b) Ni *L*-edge x-ray absorption spectra (XAS) measured at 300 K. La $M_4$ edge has been subtracted. 12 nm LNO film XAS is included for comparison.

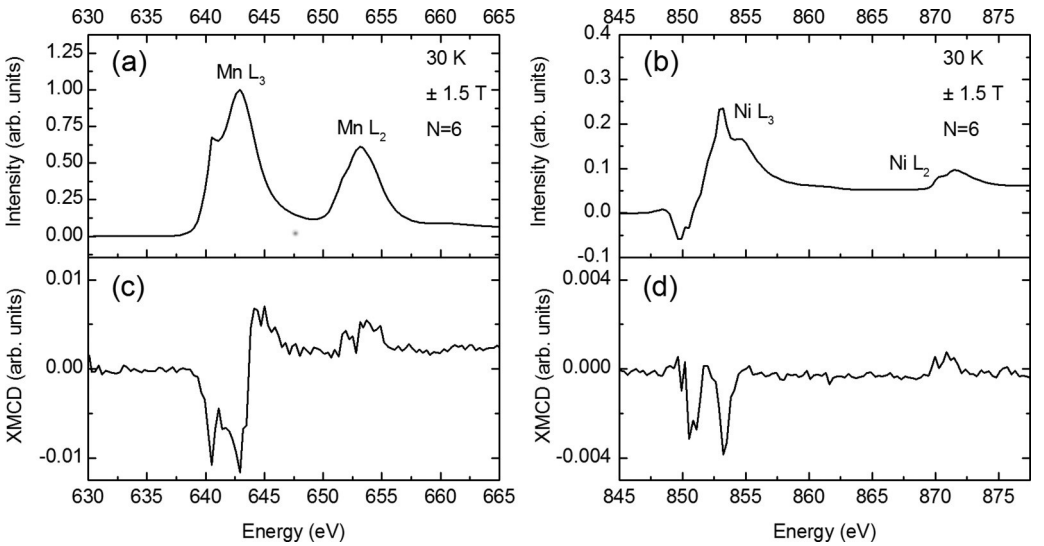


FIG. 4. (a) Mn and (b) Ni *L*-edge x-ray absorption spectra (XAS) measured at 30 K for an $N = 6$, $M = 4$ superlattice. La $M_4$ edge has been subtracted. (c) Mn and (d) Ni *L* edge x-ray magnetic circular dichroism spectra obtained from XAS difference spectra taken at ±1.5 T.

observed increased charge transfer in (111)-oriented superlat- tices [23]. The increased $Ni^{2+}$ in (111) superlattices is also correlated with more insulating transport behavior. The fact that the $Ni^{2+}$ fraction is higher for (111) superlattices and that it diminishes with *N* thickness is consistent with a polar compensation mechanism [6]. The enhanced polar compensa- tion effect has also been observed in LNO thin films [21,22]. In ($\underline{1}$11) superlattices with the thickest LNO layers ($N$ 10) and the largest fraction of $Ni^{3+}$, the transport behavior is more metallic with resistivity approaching that of a 9-nm-thick metallic LNO thin film as seen in Fig. 3(a). Therefore, the resistivity and XAS measurements are consistent with the $Ni^{2+}$ content and insulating behavior being an interfacial phenomenon.

Previously studied (001)-oriented CMO/CRO superlat- tices exhibited overall metallic behavior due to the metallicity of the CRO layer. The emergent ferromagnetism was attributed to a double-exchange interaction among interface Mn ions in the CMO mediated by itinerant electrons in the adjacent layer. In (001) LNO/CMO superlattices, systems with thicker than four unit cells of LNO exhibit metallic behavior, and hence the emergent ferromagnetism has been at least partly attributed to a double-exchange mechanism in metallic superlattices [6]. In these systems, metallic LNO possesses itinerant electrons that leak into the adjacent interfacial CMO layer resulting in a mixed $Mn^{3+}$-$Mn^{4+}$ valence, resulting in $Mn^{3+}$-$Mn^{4+}$ double exchange [5,6]. This is the same mechanism that has been identified in other metallic CMO-based superlattices [1,3,4,24,25]. However, systems with fewer than four unit cells of LNO are insulating, and their emergent ferromagnetism has been attributed to $Ni^{2+}$-O-$Mn^{4+}$ superexchange interactions [6]. In these systems, the Goodenough-Kanamori rules for electron transfer in a system with half-filled and filled $e_g$ orbitals dictate a ferromagnetic interaction [26,27]. Therefore, in our semiconducting/insulating (111) CMO/LNO superlattices, the emergent ferromagnetism is likely attributed to $Ni^{2+}$-O-$Mn^{4+}$ superexchange interactions. In Fig. 4, we show

XAS and x-ray magnetic circular dichroism (XMCD) of the Mn [Fig. 4(a)] and Ni [Fig. 4(b)] $L$-edges for an $N$ 6, $M$ 4 superlattice. The XMCD measurements were performed at 30 K in a 1.5 T magnetic field. We note that the XMCD signal reverses with a reversal of magnetic field, indicative of a real XMCD signal. The existence of $Ni^{2+}$ and $Mn^{4+}$ XMCD at 853 and 623 eV, respectively, is consistent with our results on insulating (001)-oriented LNO/CMO superlattices and with $Ni^{2+}$-O-$Mn^{4+}$ superexchange interactions [28,29].

To shed light on the origin of emergent ferromagnetism in (111)-oriented CMO/LNO superlattices, we characterized the superlattices using bulk SQUID magnetometry (Fig. 5). Figure 5(a) shows the temperature dependence of the normalized [$M$ (T)/$M$ (10 K)] magnetic moment from 10 to 300 K after field-cooling in 7 T with a 0.5 T warming field. The onset of ferromagnetism is around 200 K, as indicated by the nonlinear and sudden increase in magnetization at this temperature. We note that a precise estimate of $T_c$ in these samples is difficult from this magnetization data due to the multiple competing magnetic interactions, as is also observed in $La_2NiMnO_6$. The small feature just below 50 K is due to paramagnetic oxygen frozen onto the sample. The superlattice ferromagnetism exhibits an increasingly idealized Brillouin-type temperature dependence with increasing LNO thickness, although the temperature dependence was not fit to the Brillouin function. The saturated magnetic moment of the superlattices was determined at 10 K after field-cooling in 7 T. Measurements were performed in no overshoot mode after a wait time of 600 s to ensure SQUID magnet ramping, and hysteresis did not alter the results. Figure 5(b) shows the field dependence for an $N$ 6, $M$ 4 superlattice with a (1) $N$ 6, $M$ 4 superlattice for comparison. While the ferromagnetism arises from both Ni and Mn due to Ni-Mn superexchange, as noted above and detailed in previous work [6], we show the magnetization normalized to the number of interfacial Mn ions to enable a comparison to previous results on $CaMnO_3$-based superlattices [1,3–7]. The SQUID signal is accurate to within ~10%, which is consistent with

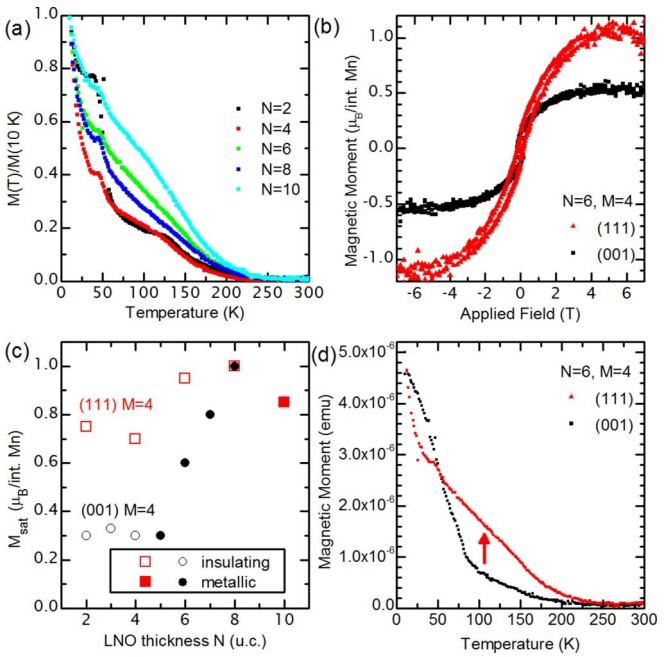


FIG. 5. (a) Temperature dependence of normalized magnetiza- tion for (111)-oriented superlattices. Magnetization is normalized by the magnetization at 10 K. Samples were field-cooled in 7 T and then warmed in 0.5 T. (b) Magnetic moment vs applied field for (111)-oriented $N$ 6, $M$ 4 superlattice after diamagnetic and paramagnetic background subtraction. Measured at 10 K after 7 T field cooling. (001) sample data are provided for comparison. (c) Sat- urated magnetic moment at 7 T and 10 K for (111) superlattices after subtraction of the high-temperature moment due to the diamag- netic substrate. (001) superlattice results are shown for comparison. Open symbols indicate the insulating LNO regime. Closed symbols indicate the metallic LNO regime. (d) Temperature dependence of magnetic moment (emu) for the same (111) $N$ 6, $M$ 4 sample and (001) comparison sample. (111)-oriented superlattice exhibits increased $T_C$ as indicated by the red arrow.

the level of noise observed in Fig. 5(b). The plot shows a significant enhancement of the saturated magnetic moment in the (111)-compared to the (001)-oriented superlattices. The (111)-oriented superlattice ferromagnetism is summa- rized in Fig. 5(c), along with the results for (001)-oriented $M$ 4 superlattices for comparison. Since the (111) $N$ 8 superlattices are insulating/semiconducting, they are most equivalently compared to the insulating (001) superlattices [i.e., $N < 5$, open symbols in Fig. 5(c)]. The moments for the (001) insulating superlattices are less than half of the saturated moment of the (111) superlattices. Therefore the (111) orientation of the interface appears to result in an enhanced ferromagnetic moment due to a largely uncompen- sated (111) CMO spin structure at the interface and stabilized by a strong $Ni^{2+}$-$Mn^{4+}$ superexchange interaction, consistent with the operative ferromagnetic mechanism in insulating (001)-oriented LNO/CMO superlattices [6]. As in the (001)- oriented superlattices, we find that $Ni^{2+}$ is confined to the interface, and we speculate that oxygen vacancies compensate $Ni^{2+}$ formation at the polar interfaces. In this model, the polar mismatch at the interface is the driving force to create oxygen vacancies, which then lead to the formation of $Ni^{2+}$ (see the

Supplemental Material [16] for more details). The metal- lic (001) superlattices ($N$ ≥ 5) have an additional double- exchange interaction that dominates for thicker $N$ [7], which is also present in the metallic (111) superlattices ($N$ > 8). It is interesting to note that the saturated magnetic moment in the (001) superlattices never exceeds that of the (111) superlattices even for $N$ > 5, thus suggesting that the (111) in- terface is close to fully uncompensated. This result, combined with the equivalent $Ni^{2+}$-$Mn^{4+}$ superexchange mechanism underlying the insulating superlattices in both orientations, leads to a saturated magnetic moment for (111) superlattices that is largely unchanged for variations in $N$ .

Enhanced ferromagnetism is evident for the (111)-oriented sample. To further understand the mechanism for the enhance- ment, the temperature dependence of the magnetization was investigated as seen in Fig. 5(d) in absolute units (emu). The $T_C$ for the (111)-oriented sample is substantially enhanced from that of the corresponding (001)-oriented sample, as can be seen by the change in concavity between 100 and 200 K between the samples. While there is a weak increase in the magnetization above 100 K for the (001)-oriented sample, the magnetization does not substantially increase until about 85 K. On the other hand, the magnetization for the (111)-oriented sample begins increasing significantly at 200 K.

## IV. DISCUSSION

The increase in $T_C$ for the (111)-oriented $N$ = 6 superlat- tice is consistent with enhanced superexchange as observed in ordered $La_2NiMnO_6$ [29,30]. Ordered $La_2NiMnO_6$ has a $T_C$ close to 300 K. However, when it is disordered, the amount of Ni-Mn bonding is reduced in favor of weaker ferromagnetic and antiferromagnetic exchange interactions. This suppresses the Ni-Mn superexchange ferromagnetism, leading to a mag- netically disordered $La_2NiMnO_6$ with $T_C$ of 140 K. This same disorder and competition between magnetic mechanisms also explains why the $N$ < 5 (001)-oriented superlattices have a suppressed transition temperature and magnetic moment in comparison with the (111)-oriented superlattices. In fact, the analogy is likely a direct one, as the shapes of the (001)/(111) temperature-dependence curves are remarkably similar to those for the disordered/ordered $La_2NiMnO_6$, respectively [29,30].

These results are consistent with the interactions previ- ously found for nickelate/manganite superlattices and Ni-Mn double perovskites. We would also expect a system with ferromagnetic and antiferromagnetic interactions to possi- bly exhibit exchange bias. For example, it is well known that (111)-oriented LNO/LMO superlattices exhibit exchange bias, likely by inducing magnetic order in the LNO layer [10,23,31]. Recently, exchange bias has been observed in (001)- and (110)-oriented LNO/LMO as well [32]. Exchange bias has also been observed in Sr-doped $La_2NiMnO_6$ as the result of Sr-induced antisite defects that lead to antiferro- magnetic antiphase boundaries [33]. Therefore, exchange bias is expected to be correlated with smooth interfaces in order for it to be attributed to emergent interfacial phenomena. We demonstrate that all of our superlattices exhibit Laue oscillations in both the XRD and XRR measurements, thus making a strong case that the observed exchange bias is not

=

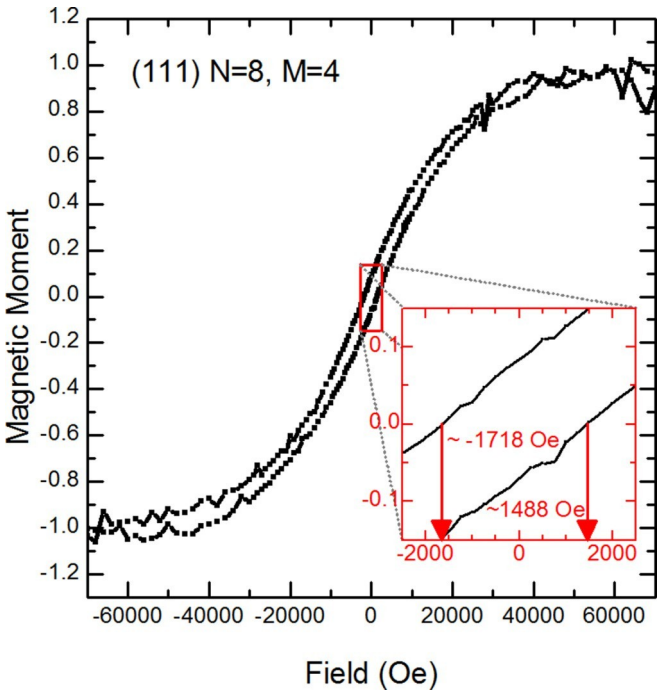


FIG. 6. Magnetic moment vs applied field with the low-field region in the inset for (111) $N$ 8, $M$ 4 superlattice. The sample was field-cooled measured at 10 K after field-cooling in 7 T.

due to surface roughness or defects (Fig. 2). Figure 6 presents results for the (111)-oriented $N$ 8, $M$ 4 superlattice after 7 T field-cooling for comparison. The hysteresis loop for the (111) $N$ 8, $M$ 4 superlattice and the inset showing the low-field region show evidence for exchange bias of 115 32 Oe. Exchange bias of this magnitude cannot be explained in terms of the SQUID remanent magnetic field, which is on the order of 20 G for Quantum Design MPMS. Furthermore, in contrast to the (111) superlattices, (001) $M$ 4 superlat- tices show no appreciable exchange bias (18 35 Oe).

Similar exchange bias is observed by Gibert *et al.* in (111)-oriented LNO/LMO superlattices but not in the (001)- oriented superlattices [10]. Theoretical results suggest this is because the LNO biasing layer is either not magnetic or only weakly magnetic in (001)-oriented LNO/LMO superlattices [10,23,31]. In LNO/LMO superlattices, the ferromagnetic LMO layer clearly is the dominant ferromagnetic layer, which is ferromagnetic in thin-film form, despite being antiferro- magnetic in the bulk [10,34]. Thus, LNO acts as the biasing layer in LNO/LMO [10]. However, in our LNO/CMO su- perlattices we believe that the antiferromagnetic CMO may bias the interfacial ferromagnetic CMO layer, which has previously been observed in CMO-based superlattices [5]. Unlike LMO, CMO maintains its antiferromagnetism in thin- film form [35]. Interestingly, however, we note that in all of these manganite-based systems, the exchange bias appears to arise despite not following the classic example of $T_N > T_C$ .

For the case of LNO/CMO superlattices, the presence of exchange bias in (111)-oriented superlattices may be due to the existence of the uncompensated CMO spin structure at the interfaces, compared to the fully compensated spin structure in (001)-oriented superlattices.

## V. SUMMARY

In summary, we have demonstrated that emergent inter- facial ferromagnetism in (111)-oriented LNO/CMO super- lattices arises from $Ni^{2+}$-$Mn^{4+}$ superexchange interactions associated with screening effects due to polar mismatch. This has been made possible due to the successful synthesis of (111)-oriented LNO/CMO superlattices with clear ordering of the superlattice periods. These superlattices exhibit in- creased resistivities compared to (001) LNO/CMO superlat- tices that are correlated with increased $Ni^{2+}$. For all (111)-oriented superlattices, the ferromagnetism is enhanced with a $T_C > 200$ K. In analogy to $La_2NiMnO_6$, this is likely the result of increased $Ni^{2+}$-$Mn^{4+}$ interactions along the (111) interfaces. The saturated magnetic moment is also enhanced compared to corresponding (001)-oriented insulating super- lattices by as much as a factor of 3 and is attributed to the largely uncompensated CMO spin structure along the (111) interface. Finally, it was demonstrated that (111)-oriented superlattices exhibit exchange bias in addition to enhanced ferromagnetism. The origin of this exchange bias is not fully understood and may be influenced by both the LNO layer and the antiferromagnetic CMO region. This work on (111)- oriented $CaMnO_3$-based magnetic heterostructures paves the way for the control of emergent magnetism at interfaces and incorporation into future spintronic applications.

## ACKNOWLEDGMENTS

This work was supported by the U.S. Department of En- ergy, Director, Office of Science, Office of Basic Energy Sci- ences, Division of Materials Sciences and Engineering under Contract No. DESC0008505. Use of the Stanford Synchrotron Radiation Light source, SLAC National Accelerator Labora- tory, is supported by the U.S. Department of Energy, Office of Science, Office of Basic Energy Sciences under Contract No. DE-AC02-76SF00515. This research used resources of the Advanced Light Source, which is a U.S. Department of Energy Office of Science User Facility under Contract No. DE-AC02-05CH11231. This research also used resources of the Advanced Photon Source, a U.S. Department of Energy Office of Science User Facility operated for the DOE Office of Science by Argonne National Laboratory under Contract No. DE-AC02-06CH11357. Part of this work was performed at the Stanford Nano Shared Facilities (SNSF), supported by the National Science Foundation under Award No. ECCS-1542152.

[1] K. S. Takahashi, M. Kawasaki, and Y. Tokura, Appl. Phys. Lett. **79**, 1324 (2001).

[2] B. R. K. Nanda, S. Satpathy, and M. S. Springborg, Phys. Rev. Lett. **98**, 216804 (2007).

[3] J. W. Freeland, J. Chakhalian, A. V. Boris, J.-M. Tonnerre, J. J. Kavich, P. Yordanov, S. Grenier, P. Zschack, E. Karapetrova, P. Popovich, H. N. Lee, and B. Keimer, Phys. Rev. B **81**, 094414 (2010).

[4] C. He, A. J. Grutter, M. Gu, N. D. Browning, Y. Takamura, B. J. Kirby, J. A. Borchers, J. W. Kim, M. R. Fitzsimmons, X. Zhai, V. V. Mehta, F. J. Wong, and Y. Suzuki, Phys. Rev. Lett. **109**, 197202 (2012).
[5] A. J. Grutter, H. Yang, B. J. Kirby, M. R. Fitzsimmons, J. A. Aguiar, N. D. Browning, C. A. Jenkins, E. Arenholz, V. V. Mehta, U. S. Alaan, and Y. Suzuki, Phys. Rev. Lett. **111**, 087202 (2013).
[6] C. L. Flint, H. Jang, J.-S. Lee, A. T. N'Diaye, P. Shafer, E. Arenholz, and Y. Suzuki, Phys. Rev. Mater. **1**, 024404 (2017).
[7] C. L. Flint, A. Vailionis, H. Zhou, H. Jang, J.-S. Lee, and Y. Suzuki, Phys. Rev. B **96**, 144438 (2017).
[8] G. Bergmann, Phys. Rev. Lett. **41**, 264 (1978).
[9] K. Ueda, H. Tabata, and T. Kawai, Science **280**, 1064 (1998).
[10] M. Gibert, P. Zubko, R. Scherwitzl, J. Iñiguez, and J.-M. Triscone, Nat. Mater. **11**, 195 (2012).
[11] T. H. Kim, D. Puggioni, Y. Yuan, L. Xie, H. Zhou, N. Campbell, P. J. Ryan, Y. Choi, J. W. Kim, J. R. Patzner, S. Ryu, J. P. Podkaminer, J. Irwin, Y. Ma, C. J. Fennie, M. S. Rzchowski, X. Q. Pan, V. Gopalan, J. M. Rondinelli, and C. B. Eom, Nature (London) **533**, 68 (2016).
[12] G. Koster, G. J. H. M. Rijnders, D. H. A. Blank, and H. Rogalla, Appl. Phys. Lett. **74**, 3729 (1999).
[13] K. Sreedhar, J. M. Honig, M. Darwin, M. McElfresh, P. M. Shand, J. Xu, B. C. Crooker, and J. Spalek, Phys. Rev. B **46**, 6382 (1992).
[14] W. Paszkowicz, J. Pitosa, S. M. Woodley, P. A. Duewski, M. Kozowski, and C. Martin, Powder Diffr. **25**, 46 (2010).
[15] S. Middey, D. Meyers, M. Kareev, E. J. Moon, B. A. Gray, X. Liu, J. W. Freeland, and J. Chakhalian, Appl. Phys. Lett. **101**, 261602 (2012).
[16] See Supplemental Material at http://link.aps.org/supplemental/10.1103/PhysRevMaterials.3.064401 for more details on growth calibrations, surface morphology measured by atomic force microscopy and La M edge subtraction in x-ray absorption spectroscopy.
[17] E. Breckenfeld, Z. Chen, A. R. Damodaran, and L. W. Martin, ACS Appl. Mater. Interf. **6**, 22436 (2014).
[18] H. Wei, J. L. Barzola-Quiquia, C. Yang, C. Patzig, T. Höche, P. Esquinazi, M. Grundmann, and M. Lorenz, Appl. Phys. Lett. **110**, 102403 (2017).
[19] R. Scherwitzl, P. Zubko, C. Lichtensteiger, and J.-M. Triscone, Appl. Phys. Lett. **95**, 222114 (2009).
[20] R. D. Sánchez, M. T. Causa, A. Caneiro, A. Butera, M. Vallet- Regí, M. J. Sayagués, J. González-Calbet, F. García-Sanz, and J. Rivas, Phys. Rev.B **54**, 16574 (1996).
[21] S. Middey, P. Rivero, D. Meyers, M. Kareev, X. Liu, Y. Cao, J. W. Freeland, S. Barraza-Lopez, and J. Chakhalian, Sci. Rep. **4**, 6819 (2014).
[22] M. Saghayezhian, Z. Wang, H. Guo, Y. Zhu, E. W. Plummer, and J. Zhang, Phys. Rev. B **95**, 165434 (2017).
[23] C. Piamonteze, M. Gibert, J. Heidler, J. Dreiser, S. Rusponi, H. Brune, J.-M. Triscone, F. Nolting, and U. Staub, Phys. Rev. B **92**, 014426 (2015).
[24] B. R. K. Nanda and S. Satpathy, Phys. Rev. B **78**, 054427 (2008).
[25] A. J. Grutter, A. Vailionis, J. A. Borchers, B. J. Kirby, C. L. Flint, C. He, E. Arenholz, and Y. Suzuki, Nano Lett. **16**, 5647 (2016).
[26] J. B. Goodenough, Phys. Rev. **100**, 564 (1955).
[27] J. Kanamori, J. Phys. Chem. Solids **10**, 87 (1959).
[28] H. Schmid and W. Mader, Micron **37**, 426 (2006).
[29] H. Guo, A. Gupta, M. Varela, S. Pennycook, and J. Zhang, Phys. Rev. B **79**, 172402 (2009).
[30] K. D. Truong, M. P. Singh, S. Jandl, and P. Fournier, Phys. Rev. B **80**, 134424 (2009).
[31] A. T. Lee and M. J. Han, Phys. Rev. B **88**, 035126 (2013).
[32] J. Zang, G. Zhou, Y. Bai, Z. Quan, and X. Xu, Sci. Rep. **7**, 10557 (2017).
[33] Y. Guo, L. Shi, S. Zhou, J. Zhao, C. Wang, W. Liu, and S. Wei, J. Phys. D **46**, 175302 (2013).
[34] H. Tanaka, N. Okawa, and T. Kawai, Solid State Commun. **110**, 191 (1999).
[35] C. L. Flint, A. J. Grutter, C. A. Jenkins, E. Arenholz, and Y. Suzuki, J. Appl. Phys. **115**, 17D712 (2014).